Characterization of surface graphitic electrodes made by excimer laser on CVD diamond

M. De Feudis [a,b,*], A.P. Caricato [a,b,c], G. Chiodini [a], M. Martino [a,b,c], E. Alemanno [b], G. Maruccio [b,c], A.G. Monteduro [b,c], P.M. Ossi [d], R. Perrino [a], S. Spagnolo [a,b]

[a] INFN National Institute of Nuclear Physics, 73100 Lecce, Italy
[b] Department of Mathematics and Physics, University of Salento, 73100 Lecce, Italy
[c] CNR-Nanotec, 73100 Lecce, Italy
[d] NEMAS, Department of Energy and NEMAS, Polytechnic of Milan, 20133 Milan, Italy

In this work graphitic structures were fabricated on high quality polycrystalline CVD diamond by using a UV laser beam ($\lambda = 193$ nm). Two different kinds of structures were realized on diamond to study the evolution from di-amond to graphite at different irradiation conditions (spot like structures) and to study their electrical transport properties (strip like structures). The graphitic structures were characterized structurally and morphologically by micro-Raman spectroscopy and atomic force microscopy. The electrical properties were evaluated using the transmission line model. Finally, a full carbon detector was built and tested showing good nuclear detection properties.

Keywords:
Diamond detectors
Diamond graphitization
Graphitic electrodes
Excimer laser

1. Introduction

CVD diamond material is an attractive choice as ionizing particle sensor for extremely demanding applications ranging from high energy physics to radiotherapy and nuclear fusion reactors. The realization of reliable, radiation-hard and polarization free ohmic contacts on diamond is one of the crucial steps to fulfill. In addition to this, there is a growing interest in full-carbon sensors for nuclear physics experiments (such as active carbon targets [1]) and for applied physics (such as biochemical sensors [2]). It was shown that metal-less contacts fabricated by laser writing techniques present an ohmic behavior and are polarization free [3]. Moreover, a diamond detector with graphitic contacts was irradiated with a total fluence of about $2.5 \cdot 10^{15}$ protons/cm^2 and turned out to be radiation resistant [4]. In this work it is presented a more systematic fundamental study to better understand the previous promising results in order to exploit the laser graphitization technique for the above mentioned applications. In this respect, the laser-induced graphitization process on diamond surfaces was systematically studied by realizing two different kinds of structures (spots and strips), changing the experimental irradiation conditions (beam energy density, number of laser pulses and cycles of scans) and applying different complementary analysis techniques in order to evaluate the morphological, structural and electrical properties of the realized structures. This comprehensive experimental study allowed to understand the interplay between the graphitization and ablation processes and to measure quantitatively the electrical resistivity and the geometrical parameters of the graphitic contacts. Subsequently, thanks to this study, a full carbon detector was realized demonstrating the good charge collection properties of the graphitic electrodes. In this respect, twenty strip electrodes were realized on a detector grade polycrystalline CVD diamond which were tested with 120 GeV pion during a testbeam at CERN, in Geneva.

2. Manufacturing of graphitic spots and strips

From the literature it is well known that when a laser radiation hits a diamond surface, with appropriate values of wavelength and energy density, the localized heating, induced by electron thermalization, could overcome the potential barrier of the diamond-graphite transition, which is $T > T_g \approx 700$ °C in air [5]. In particular, if the energy density is large enough, the diamond photothermal modification occurs already at the first laser shot. Then, due to the different physical properties of graphite with respect to diamond and in particular the higher absorption coefficient, the other laser shots can induce graphite ablation ($T = T_S \approx 4000$ °C). Moreover, if the laser fluence is high enough, the surface graphitization and ablation can occur within a single laser shot: the surface graphitization can be induced by the leading part of the laser pulse followed by the ablation of the graphitic material by the rest of the

* Corresponding author at: INFN National Institute of Nuclear Physics, 73100 Lecce, Italy.
E-mail address: mary.defeudis@le.infn.it (M. De Feudis).

Article history:
Received 1 December 2015
Received in revised form 7 February 2016
Accepted 5 March 2016
Available online 9 March 2016

laser pulse. Understanding the physical evolution and the interplay between the photothermal diamond graphitization and graphite ablation phenomena it is crucial to have a good control of the process and optimize the realization of ohmic contacts on the diamond surface. For this reason, two types of graphite structures were realized on CVD thermal grade polycrystalline diamond of dimensions $10\times 10\times 0.25$ mm^3 with different aims: graphitic spots, to study the physical evolution of the graphitization process, and graphitic strips, to find the optimal irradiation parameters to create good and reliable ohmic contacts. The experimental setup is illustrated in a simple schematic picture Fig. 1. The key elements of the graphitization process are an excimer laser, to produce an UV radiation highly absorbed by the diamond material, and a focusing optical system. For the realization of the two graphitic test structures on sample several combinations of laser parameters were used with a fixed laser frequency (10 Hz). In particular, the spots were realized using different numbers of laser pulses (N = 1, 2, 4, 8, 25, 40, 50 and 100) and fluence values (F = 2, 5 and 7 J/cm^2), while the strips were realized using different numbers of up-and-down scans (C = 1/2, 1, 2, 6, 8, 10 and 12, where C = 1/2 corresponds to one up scan) and fluence values (F = 2, 3, 5 and 7 J/cm^2). The laser scans velocity was fixed at $\upsilon = 0.2$ mm/s for the strips. In Fig. 2 is reported a picture of the graphitized CVD thermal grade polycrystalline diamond. The unirradiated sample was a CVD thermal grade polycrystalline diamond (TM100) provided by Element Six Ltd (UK) of dimensions $10 \times 10 \times 0.25$ mm^3. This sample was a material doped with boron and its most important properties are listed here: thermal conductivity >1000 W/(mK) @293 K, bulk and surface resistivity equal to 1×10^{10} Ωm and 1×10^{8} Ωm respectively, roughness after the surface polishing of one side <50 nm (graphitized surface) and after lapping of the other side <250 nm.

A preliminary inspection with an optical microscope permitted a selection of the structures to investigate both for good graphitization homogeneity along all the graphitized areas and for not excessive ablation phenomenon. The selected test structures are reported in this work: spots realized with F = 5 J/cm^2 and N = 1, 2, 4, and 8 and strips realized with F = 5 and 7 J/cm^2 and C = 2, 6 and 8.

3. Characterization of graphitic spots and strips

3.1. AFM and micro-Raman analysis of graphitic spots

Generally, at the first stage of the laser-induce process (few laser pulses, at least just one) the diamond graphitization results in a bump on the surface profile due to the mass density difference between the two carbon phases ($\rho_{diamond} = 3.5$ g/cm^2 and $\rho_{graphite} = 1.9$ g/cm^2) [5]. The next pulses, overlapping with the previous ones, induce a continuous

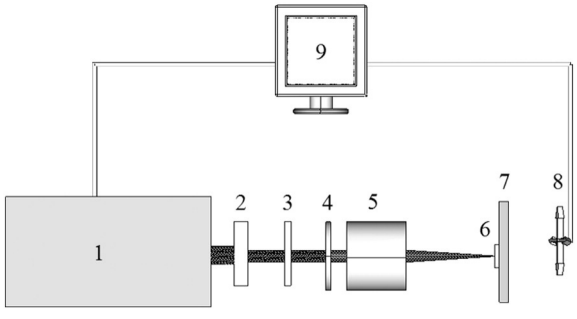

Fig. 1. Scheme of the experimental setup for the diamond graphitization. It was composed by an ArF excimer laser (1) which produced a UV radiation (wavelength $\lambda = 193$ nm and pulse duration $\tau = 20$ ns), a rectangular aperture (1×1 cm^2) (2) and a variable iris (4) to reduce the beam size, an energy attenuator (3) to modify the laser energy, and a 15× UV objective lens (5) to focus the radiation on the diamond surface (6). The diamond and its holder (7) were fixed on two submicrometric motorized translation stages (8) for the movement in the X–Y plane perpendicular to the beam direction. A LabVIEW software (9) was used to remotely control at the same time the laser and stages machines.

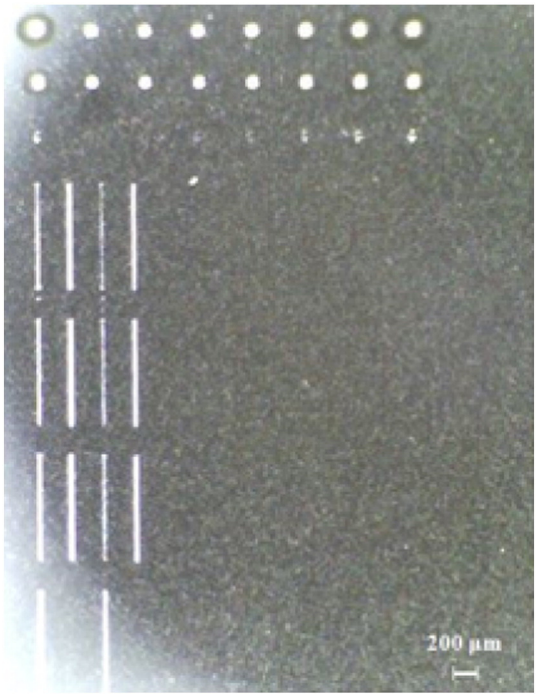

Fig. 2. Laser-induced graphite structures on CVD thermal grade polycrystalline diamond surface. The graphitic structures were realized with several combinations of the irradiation parameters (laser energy density and number of pulses). The spot diameter was 130 ± 10 µm, while the strip width was 35 ± 5 µm. The strip length was 1 mm.

transformation of the surface profile due to the simultaneous occurrence of the graphitization and ablation processes. In order to study the laser induced modification of the diamond surface profile, atomic force microscopy (AFM) investigations were carried out using a Park System Xe-70 in non-contact mode, equipped with a tip of silicon nitride with radius of curvature <10 nm. The AFM scans were performed on area of 20×20 µm^2. Fig. 3 shows the physical evolution of the average height of the spot structures obtained after laser-diamond interaction with respect to the number of pulses obtained by AFM measurements. Positive height values were found for N = 1 and 2, corresponding respectively to 108 ± 3 nm and 75 ± 3 nm, and negative height values for N = 4 and 8, corresponding respectively to −8 ± 1 nm and −106 ± 1 nm, where the zero level refers to the flat surface of unirradiated diamond [6]. This means a swelling phenomenon up to two pulses followed by a crater formation phenomena increasing the number of laser pulses. In

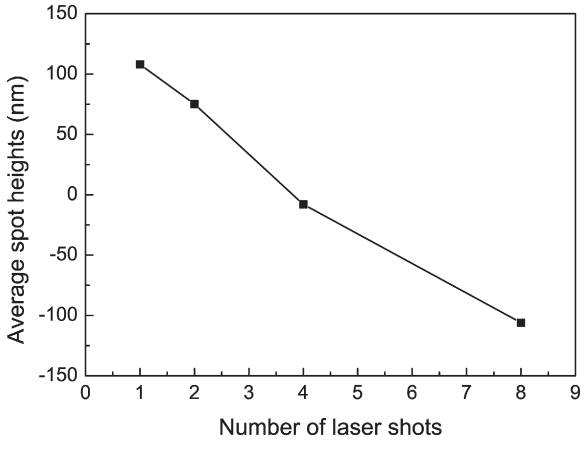

Fig. 3. Average height of the spot structures obtained with a laser fluence of 5 J/cm^2 as a function of the number of laser shots [6].

particular, the first pulse creates the graphite bump, the second pulse induces a partial ablation of the visible graphitized zone, and the next pulses generate craters with increasing depth as a result of the dominant ablation with respect to graphitization. Fig. 4 shows an AFM image of the crater generated by eight overlapped laser pulses. The image is taken on the boundary between the irradiated diamond surface and the unirradiated adjoining zone (zero level). The overall trend of the spot average heights is almost linear with the number of pulses, in agreement with literature data [5]. However, studies on graphitic spots and strips demonstrated that for any number of pulses, below the ablated layer of diamond, a graphitic layer is present.

In order to investigate the structural nature and evolution of the bumps and craters micro-Raman spectroscopic analysis was performed on these test structures. The measurements were realized using a Renishaw InVia Raman Microscope, with an Ar + laser ($\lambda = 514.5$ nm) focused by a 50× optical objective (Leica, Germany) to a spot of 1 μm diameter on the sample surface. The backscattered light, collected by the same objective, was analyzed by a microscope equipped with a holographic Notch filter (cutoff at 100 cm^{-1}), a 1800 lines/mm diffraction grating and a thermoelectrically cooled RenCam CCD detector. The wave-number resolution was 0.5 cm^{-1} in the range from 100 to 8000 cm^{-1}. Raman spectra were taken in the center of each graphitic structure. In literature, the Raman characterizations performed on CVD diamond samples with the same excitation associate a sharp peak at 1332 cm^{-1} (d peak) to carbon in diamond phase and a broad peak at 1580 cm^{-1} (G peak) to carbon in graphite phase. The intensity ratio of the two peaks indicates how much of each carbon phase is present on the surface [7]. Furthermore, in any carbonaceous material the graphitic phase presence with different degrees of disorder is associated also to other two peaks: the peak at 1350 cm^{-1} (D peak) and at 2700 cm^{-1} (2D peak). A micro-Raman spectrum of the unirradiated diamond is reported in Fig. 5. It shows a narrow d peak centered at 1332 cm^{-1} and a G band extending from about 1450 cm^{-1} to 1650 cm^{-1}. The sharp and well defined d peak is expected for a diamond material, while the G band is most likely due to the presence of graphitic carbon structures in CVD diamond [8]. In Fig. 6 the micro-Raman spectra of laser-induced spot-like structures with a laser fluence of 5 J/cm^2 at different number of laser pulses are displayed, while in Table 1 the relative intensity in a.u. of the d and G signals, associated to diamond and graphite phases respectively, are reported together with their ratio. It is possible to note that the spots created with one or two laser pulses show no evidence of any diamond phase while, increasing the number of laser pulses the d peak is again visible together with the G peak whose intensity is reduced. The lack of the d peak for spot with N = 1 and 2 in the spectroscopic measurement means that the graphitic bump height must be thick at least as much as the micro-Raman sampling depth (50 nm for $\lambda = 514.5$ nm [9]) consistent with the heights estimated by AFM analysis. Conversely, a diamond peak is expected in correspondence to spots with craters due to competitive ablation process. Together with the G peak, also the D peak of graphitic phase is constantly present in the spectra of all the spots. In particular, it is clearly visible that for the spot N = 1, where the diamond phase is absent, the D peak is broad and well defined; while increasing the number of pulses, the D peak exhibits a reduction of the relative intensity as opposed to the growth of the peak d. The constant presence of the G and D peaks confirms that both after the dominant diamond graphitization process (swelling phenomenon) and after the dominant graphite ablation process (crater formation phenomenon) the presence of trigonally coordinated carbon (graphite) is always true on the surfaces of the spots. It is worth to report that to obtain the peak intensity values of the different carbon phases no subtraction operation by baseline was done. The aim of micro-Raman analysis in this work was to investigate the structural nature and the evolution of the graphitization and ablation laser-induced processes by the valuation of the presence or absence of the different phases of carbon, and in particular, where possible, to define a trend of the behavior of the irradiated diamond surface to changing experimental parameters.

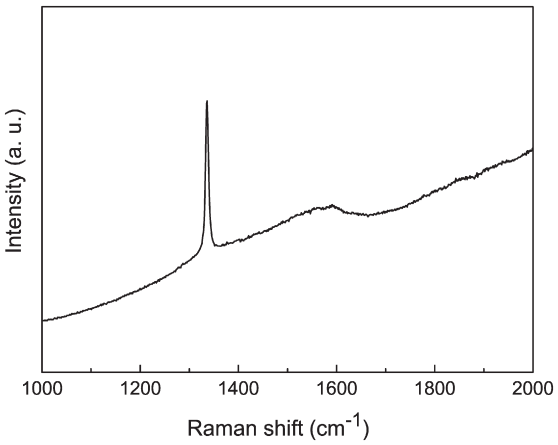

Fig. 5. Micro-Raman spectrum of unirradiated diamond.

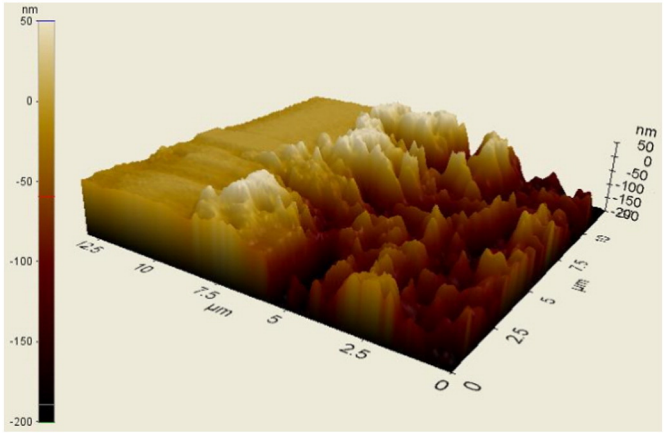

Fig. 4. AFM image of the graphitic spot boarder realized at laser fluence of 5 J/cm^2 and 8 overlapped pulses.

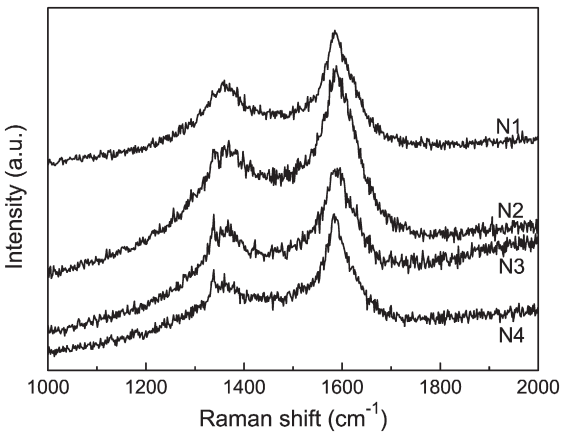

Fig. 6. Micro-Raman spectra of laser-induced spot-like structures with a laser fluence of 5 J/cm^2 at different number of laser pulses: N = 1, 2, 4, 8.

Table 1
Relative intensities and intensity ratio of the d and G Raman peaks for spots (upper half) and strips (bottom half) like laser induced structures.

	d intensity (a.u.)	G intensity (a.u.)	d/G intensity ratio
Spots			
F5N1	≈0	6.0×10^{2}	≈0
F5N2	≈0	1.0×10^{3}	≈0
F5N4	6.5×10^{2}	8.0×10^{2}	8.1×10^{-1}
F5N4	4.0×10^{2}	6.5×10^{2}	6.2×10^{-1}
Strips			
F7C2	1.2×10^{3}	2.0×10^{3}	6.0×10^{-1}
F7C6	≈0	2.6×10^{3}	≈0
F7C8	7.5×10^{2}	1.0×10^{3}	7.5×10^{-1}
F5C6	2.3×10^{3}	2.8×10^{3}	8.2×10^{-1}
F5C8	2.7×10^{3}	1.2×10^{3}	2.3

3.2. Micro-Raman and electric measurements of graphitic strips

In Figs. 7 and 8 are shown the micro-Raman spectra of the strip-like structures realized with a laser fluence of 7 and 5 J/cm ^{2} respectively, while in Table 1 the relative intensities of the main peaks are reported together with their ratio. In particular, in Fig. 7 are presented three micro-Raman spectra related to the strips realized with laser fluence F = 7 J/cm ^{2} and number of scans C = 2, 6 and 8: a progressive decrease of the d peak intensity moving from two complete up-and-down scans (C = 2) to six complete up-and-down scans (C = 6) is shown. On the other and, the G peak intensity increases with the increase of up-and-down scans (from C = 2 to C = 6). Similarly to the spot structures, this is due to the graphitization swelling phenomenon. For C = 8 the d diamond peak appears again and the G graphite peak is reduced. As before, this behavior is ascribed to a substantial ablation phenomenon and to a continuous graphitization process. The combination of laser parameters F = 7 J/cm ^{2} and C = 6, due to abundance of carbon in graphitic phase (a high G peak and a little pronounced D peak) and the absence of diamond phase (d peak), seems to be the most interesting one for the realization of conductive layers on diamond surface for nuclear detector and bio-sensor applications. It is also interesting to evaluate the micro-Raman spectra of the strip-like structures realized with laser fluence of F = 5 J/cm ^{2} and number of laser scans C = 6 and 8 (Fig. 8). Both show a definite presence of d and G peaks. In particular, comparing the intensity values of d peak among the strips realized at same number of laser scans C = 6 or 8 but with different laser fluence F = 5 and 7 J/cm ^{2} (Table 1) it is possible to note that the diamond peak presents a considerable fluctuation of intensity, confirming that once the graphitization process is started the ablation phenomenon takes place simultaneously and it is very sensitive to variations in energy. In addition, it is worth to report that for all the micro-Raman spectra of the strips (Figs. 7 and 8) the D peak is constantly visible and it completes the presence of trigonally coordinated carbon in its different phases, similarly to the case of the spots (Fig. 6). This is always true for all the strip-like structures realized at the several combinations of the irradiation parameters (laser fluences F = 5 and 7 J/cm ^{2} and scan cycles C = 2, 6 and 8).

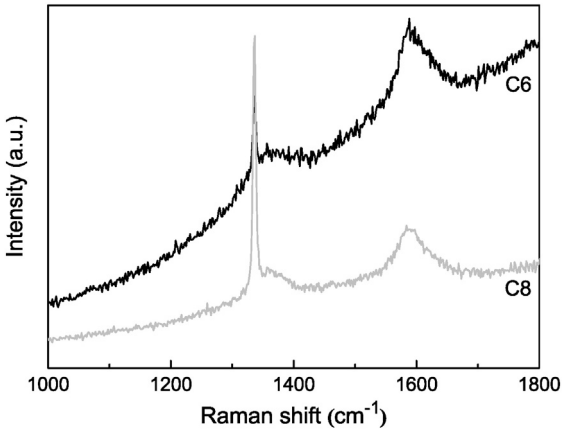

Fig. 8. Micro-Raman spectra of laser-induced strip-like structures realized with a laser fluence of 5 J/cm ^{2} at different number of laser scan cycles: C = 6, 8.

The most promising strip-like structures (those which had shown the high G peak intensities) were electrically characterized. In particular, the considered structures were that ones realized with F = 5 and 7 J/cm ^{2} and C = 6 and 8. The electrical characterization was performed using a probe station composed by two probes with tungsten tips of 40 μm in diameter, hooked to two micromanipulators for 3D movements and a by labVIEW software to control a Yokogawa 7651 programmable DC source, a SR570 low noise current preamplifier and a HP34410 digital multimeter. The ohmic nature of the graphitic strips were verified by measuring the current–voltage curves. An accurate method, based on the transmission line model (TLM) [10] was used to evaluate the electrical resistivity of the strips.

In particular, by measuring a current–voltage (I–V) curve among probe contacts placed at an increasing distance d along one strip, it is possible to extract the total resistance R_T from each I-V curve. Thus, the resistivity can be estimated from the dependenc of the total resistance R_T on the distance d between the contacts, which is expected to

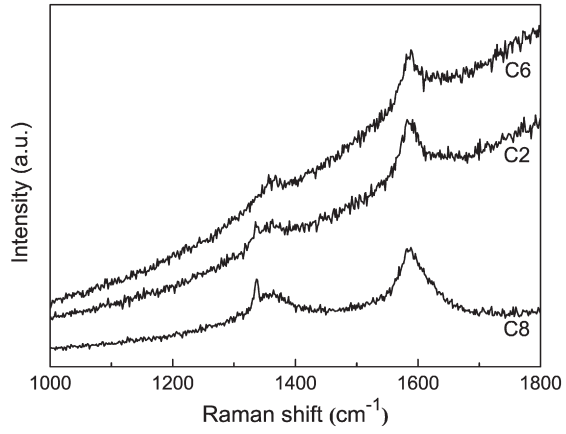

Fig. 7. Micro-Raman spectra of laser-induced strip-like structures realized with a laser fluence of 7 J/cm ^{2} at different number of laser scan cycles: C = 2, 6, 8.

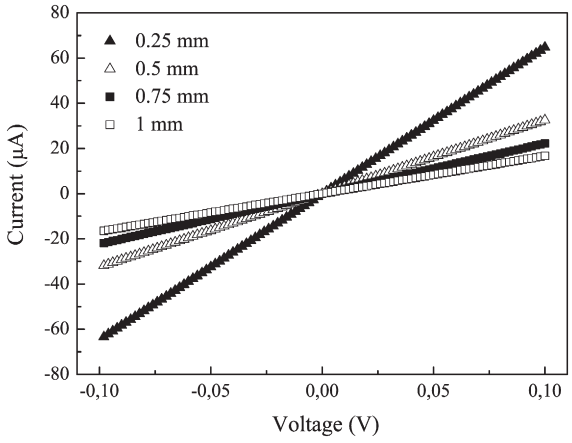

Fig. 9. Current–voltage characteristics recorded along the graphitic micro-strip realized with a laser fluence of 7 J/cm ^{2} and 6 laser scan cycles at different probe distance d: 0.25 mm (solid triangles), 0.5 mm (empty triangles), 0.75 mm (solid squares) and 1 mm (empty squares).

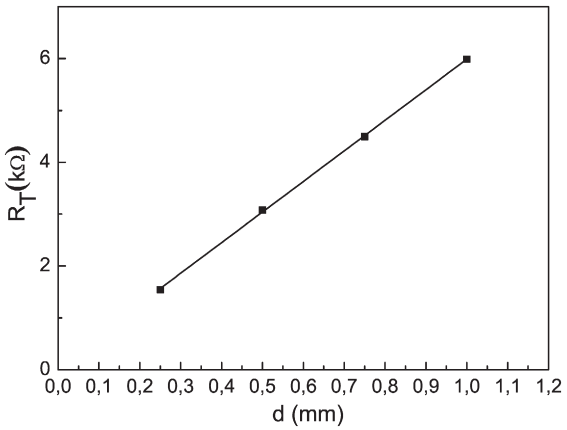

Fig. 10. Total resistance versus the distance between the contacts for the graphitic microstrip realized with a laser fluence of 7 J/cm ^{2} and 6 up-down scans.

be linear for homogeneous strips according to the equation:

$$R_T = 2R_C + \frac{\rho d}{wt}, \quad (1)$$

where R_C is the probe contact resistance and ρ, w and t are, respectively, the electrical resistivity, the width and the thickness of the strips. Fig. 9 shows typical I–V curves measured on a graphite strip (F = 7 J/cm ^{2}; C = 6) for a distance d varying from 0.25 mm to 1 mm. Each curve exhibits an almost linear trend which allows extrapolating the electrical resistance R_T value by means of a linear fit. In Fig. 10 the obtained dependence of R_T on the distance d is shown, and the graphite resistivity ρ in addition to the probe contact resistance R_C were calculated by the slope of a linear fit based on Eq. (1), after measuring the strip geometrical parameters. The planar dimensions of the strips were measured by the optical image of the strip (Fig. 2), while its thickness was estimated using AFM analysis, after a thermal annealing treatment, which removed the graphitic layer by oxidation reaction (T = 600 °C, for 150 min, in air) [11]. Knowing the average height of every graphite bump before the annealing treatment, and measuring the crater average depth after that, the total thickness was determined by adding the two values. The measured and estimated geometrical parameters together with the corresponding calculated electrical resistivity values are reported in Table 2.

The obtained electrical resistivity values for the strips are consistent with the expected one for graphite $\rho \approx 10^{-5} - 10^{-6}$ Ωm [3,5]. In particular, the strip with the lowest value of electrical resistivity $\rho = (4.0 \pm 0.8)10^{-5}$ Ωm was realized with F = 7 J/cm ^{2} and C = 6 (probe contact resistance $R_C = 92$ Ω). This structure was that one with the only graphite phase and without diamond phase (micro-Raman analysis), therefore, with the greatest quantity of graphite.

Table 2
Geometric parameter (length l, width w, thickness t) and resistivity values (ρ) of the graphitic strips realized at different irradiation fluence values (F = 5 and 7 J/cm ^{2}) and laser scan cycles (C = 6 and 8).

Strips	l (m)	w (m)	t (m)	ρ (Ωm)
F5C6	1×10^{-3}	3×10^{-5}	1.81×10^{-7}	7.5×10^{-5}
F5C8	1×10^{-3}	3×10^{-5}	1.7×10^{-7}	9×10^{-5}
F7C6	1×10^{-3}	4×10^{-5}	1.69×10^{-7}	4.0×10^{-5}
F7C8	1×10^{-3}	4×10^{-5}	2.26×10^{-7}	5.5×10^{-5}

4. Characterization of a full carbon strip detector

A diamond detector is a solid state detector working like an ionization chamber. The low thermal carrier generation, even at room temperature, allows operating the intrinsic diamond as a detector, without any needs of a diode structure to deplete the carriers and limit the thermal generation current. The bulk and surface dark currents of diamond sensors are ≈1 pA/cm ^{2} for a typical electric field of 1 V/μm. The charge collection is very fast, more than 100 μm/ns in velocity saturation regime [12]. Ohmic contacts are necessary to apply the electric drift field and collect the generated charge in a reproducible way. The best combination of laser irradiation parameters (see third row of Table 2) were considered as starting point for the realization of electrical contacts to fabricate the graphitic electrodes for a full carbon nuclear detector prototype. The used sample was a CVD detector grade polycrystalline diamond (EL) provided by Element Six Ltd. (UK) of dimensions 5 × 5 × 0.325 mm ^{3}. This sample has a limited quantity of impurities (boron concentration <1 ppb and nitrogen concentration <50 ppb) and the roughness of both the surfaces after the polishing < 20 nm. Twenty graphitic strips with a width of about 100 μm and a length of about 3.5 mm were realized on one sample side and a 3.5 × 3.5 mm ^{2} graphitic pad on the other side (Fig. 11). Both the strips and the pad were made with the same laser irradiation parameters (fluence F = 7 J/cm ^{2} and scan cycles C = 6), but with a gap of about 68 μm for the strips and a geometrical overlap of 50% between adjacent laser scans for the pad. In principle, the strip processing optimization could depend on diamond type, quality and surface polishing. Nevertheless, the graphitization-ablation process, in this case, is expected not strongly dependent on diamond type after the first graphitization layer is formed [13].

4.1. Electric measurements

To test the uniformity of the graphitization process, the electric resistance was measured with the TLM method for various graphite electrodes, for different incremental distance (five steps of 100 μm in both directions for four strips and five steps of 500 μm in one directions for six strips) and for different zones of the same graphite strip (the group of measurements of 100μm step was done starting from 100 μm from the strip border and repeated again starting from the strip center). In Fig. 12 (left scale), the diamond electric resistance measurements of one graphitic strip are shown as a function of the contact separation and its linear fit provides the electric resistance per unit length (1.5 MΩ/m) and the graphite/probe contact resistance (R_C = 225 Ω). Measuring the electrode width of 100 μm and assuming an electrode thickness of 0.169 μm like the sample F7C6 (our best guess from Table 2), the resistivity is evaluated to be about 2.5 × 10^{-5} Ωm and it have to be compared

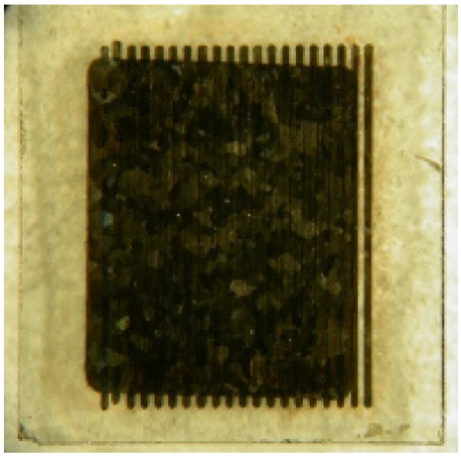

Fig. 11. Full carbon detector: CVD detector grade polycrystalline diamond sample graphitized on both surfaces with 20 strips on the front side and a pad on the back side.

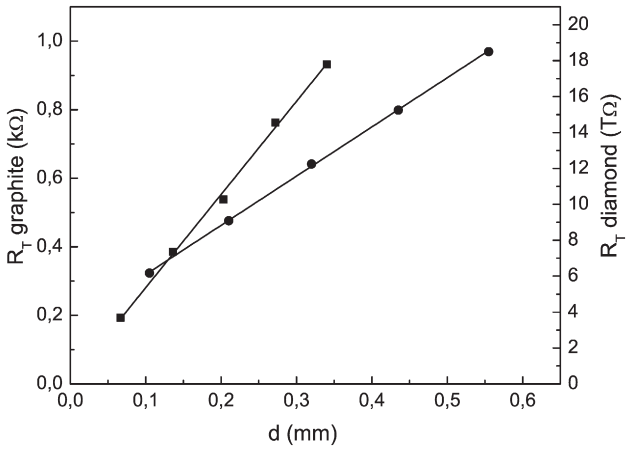

Fig. 12. Total resistance vs distance between the contacts placed on one graphitic strip (dots) and on two different graphite electrodes (squares).

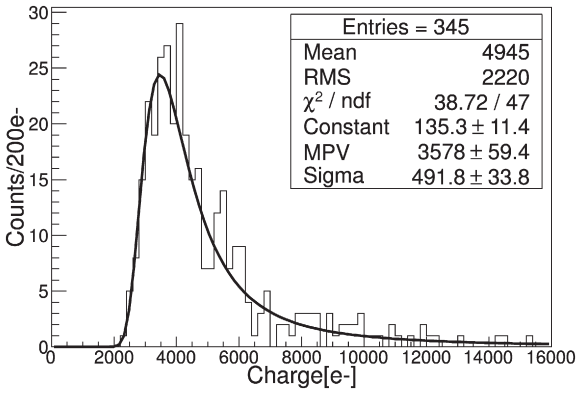

Fig. 13. Charge distribution of the graphitized diamond detector with a Landau curve fit superimposed as measured with ultra-relativistic pions.

with 4×10^{-5} Ωm, value of the sample F7C6 (Table 2). The relative standard deviation of the measured resistances per unit length, corresponding to a total of 24 measurements, turn out to be about 15% and it is dominated by the systematic error related to the reproducibility of the graphite/probe contacts (for these, a variation from 0 to 250 Ω were observed). It is possible to conclude that the electrical resistance uniformity of the graphitization process is much better than 15%. The electric isolation between strips can also be measured with the TLM method by fixing the first contact on a graphitic strip and changing the position of the second contact on the subsequent graphite electrodes. Also in this case, an almost linear behavior was observed over the voltage range investigated, from −10 V to +10 V, which suggests an ohmic nature for the graphite/diamond contact (Fig. 12 right scale). The effective diamond bulk electric resistance was also evaluated contacting a central graphitic strip on one side and the graphitic pad on the opposite side and determining the current–voltage curve. A linear behavior was observed over the voltage range between −20 V and 20 V and using Eq. (1), with $R_C \approx 0$, $w \times d = 0.1 \times 3.5\ mm^2$ respectively electrode width and length, and $t = 0.325$ mm diamond thickness, thus the diamond resistivity turn out to be $3 \pm 2 \times 10^{11}$ Ωm in a dark box. It is worth to report that the measured diamond resistivity is an order of magnitude lower in presence of light.

4.2. Response to an ionizing particle

In order to verify the charge collection properties of the graphitic electrodes, the device response to nuclear radiations was investigated in a testbeam at CERN SPS (Super Proton Synchrotron) by means of pions with an energy of 120 GeV, a rate of about 50 kHz and a beam spot of about 5 cm^2. An ultrarelativistic pion creates an average number of electron–hole pairs of about 36 e-h/μm. Anyway, the free charge carrier lifetimes are limited by the presence of trapping defects like impurities and grain boundaries. Consequently, the charge collection efficiency is strongly correlated with crystal quality. One of the main parameter used to assess the quality of CVD diamond as particle detector is the Charge Collection Efficiency (CCE) defined by the ratio between the collected and created charge due to the passage of a ultra-relativistic charged particle crossing the sensor orthogonally. In order to apply the high voltage bias, the diamond sensor was mechanically kept by two gold arms soldered to the electric contacts of a SMA connector. The electromagnetic shielding was obtained packaging the detector in a small anodized aluminum box. Two diamond detectors with traditional metal contacts were placed up-stream and down-stream the device under test in order to select events with particle crossing the fiducial area with high probability. The temporal coincidence between the signals of the two reference detectors triggered the recording of the pulse response of the detector under test. The diamond detector signal was amplified by a fast charge amplifier with a peaking time of about 5 ns and digitized by a fast waveform digitizer of 500 MHz bandwidth, a 5 G Sample/s sampling speed and a 12 bit Analog-to-Digital conversion. The electronic chain, made of the charge sensitive amplifier plus the digitizer, was calibrated by injecting of a known charge $Q_{cal} = C_{cal}V$ using a AC coupled calibration capacitance C_{cal} of about 1 pF and a voltage square generator of amplitude V = 10 mV and 1 kHz frequency. The injected charge uncertainty is about 10% and it is dominated by the uncertainty on the value of C_{cal}. Fig. 13 shows the charge spectrum of the graphitized detector obtained after the calibration of the electronic chain. The average collected charge is about 5000 ± 500 electrons, corresponding to a CCE of 42 ± 4%. This CCE value is reasonably in agreement with what reported on the supplier datasheet, which is expected to be higher than 36% for a diamond thickness of 500 μm.

5. Conclusion

The intent of this work was to optimize the experimental parameters for realization of graphitic ohmic contacts on diamond surface by UV laser irradiation in order to realize full carbon nuclear particle detector. Spot-like and strip-like graphitic test structures realized on diamond with different laser energy density and number of pulses or scan cycles allowed to get insight on the graphitization process and select the best experimental conditions to realize good ohmic contacts. This was possible thanks to an extensive and exhaustive characterization work employing micro-Raman Spectroscopy, Atomic Force Microscopy and Current–Voltage measurements. These techniques enabled investigating the evolution from diamond to graphite phase, the morphology of the irradiated diamond and the electrical resistivity of the graphitic structures. In particular, the graphitic strip realized with a fluence of 7 J/cm^2 and 6 laser scan cycles turn out to have the lowest electrical resistivity $\rho = 4.0 \times 10^{-5}$ Ωm. This combination of the laser irradiation parameters was used to built a highly segmented full carbon detector prototype and subsequently it was tested with a 120 GeV pion beam at CERN infrastructures showing good nuclear detection performances. This work paves the way to the realization of position sensitive full carbon nuclear detectors. Work is in progress to fully characterize the diamond microstrip detector in terms of efficiency and space resolution.

Acknowledgments

We acknowledge the dr. V. Russo (Polytechnic of Milan) for the valuable scientific consulations, and M. Corrado, G. Fiore, C. Pinto and P. Mazzotta (INFN section of Lecce) for setting up the experimental apparatus and the instrumentations.

References

[1] M. Raggi, V. Kozhuharov, Proposal to search for a dark photon in positron on target collisions at DAΦNE Linac, Adv. High Energy Phys. (2014), ID959802.

[2] F. Picollo, A. Battiato, E. Carbone, L. Croin, E. Enrico, J. Forneris, S. Gosso, P. Olivero, A. Pasquarelli, V. Carabelli, Development and characterization of a diamond-insulated graphitic multi electrode array realized with ion beam lithography, Sensors 15 (2015) 515–528.

[3] E. Alemanno, M. Martino, A.P. Caricato, M. Corrado, C. Pinto, S. Spagnolo, G. Chiodini,
R. Perrino, G. Fiore, Laser induced nano-graphite electrical contacts on synthetic polycrystalline CVD diamond for nuclear radiation detection, Diam. Relat. Mater. 38 (2013) 32–35.

[4] E. Alemanno, A.P. Caricato, G. Chiodini, A. Corvaglia, G.A.P. Cirrone, G. Cuttone, M. Dinardo, P. Dangelo, M. De Napoli, G. Fiore, S. Kwan, S. Malvezzi, A. Leone, M. Martino, D. Menasce, L. Moroni, D. Pedrini, R. Perrino, N. Randazzo, C. Pinto, R. Rivera, S. Spagnolo, V. Sipala, C. Tuvé, L. Uplegger, Radiation damage of polycristalline diamond exposed to 62 MeV protons, Nucl. Inst. Methods A 730 (2013) 152–154.

[5] V.I. Konov, Laser in micro and nanoprocessing of diamond materials, Laser Photonics Rev. 6 (2012) 739–766.

[6] M. De Feudis, A.P. Caricato, M. Martino, E. Alemanno, P. Ossi, G. Maruccio, A.G. Monteduro, M. Corrado, Realization and characterization of graphitic contacts on diamond by means of laser, Proceeding of the IV National Workshop on Plasmi Sorgenti Biofisica e Applicazioni PSBA, ISBN: 9788883051081, 2015 Lecce (Italy).

[7] A.T. Collins, in: A. Paoletti, A. Tucciarone (Eds.), The physics of diamond, IOS Press, Oxford, UK, 1997.

[8] L. Nistor, V. Ralchenko, I. Vlasov, A. Khomich, R. Khmelnitskii, P. Potapov, J. Van Landauyt, Formation of amorphous carbon and graphite in CVD diamond upon an-nealing: a HREM, EELS, Raman and optical study, Phys. Status Solidi A 186 (2)(2001) 207–214.

[9] Z. Ni, Y. Wang, T. Yu, Z. Shen, Raman spectroscopy and imaging of graphene, Nano Res. 1 (2008) 273–291.

[10] G.K. Reeves, H.B. Harrison, Obtaining the specific contact resistance from transmis-sion line model measurements, IEEE Electron Device Lett. 3 (1982) 111–113.

[11] V.V. Kononenko, T.V. Kononenko, S.M. Pimenov, V.I. Konov, P. Fischer, V. Romano, H.P. Weber, A.V. Khomich, R.A. Khmelnitskiy, V.N. Strekalov, Laser induced structure transformations of diamonds, Proceeding of Laser Processing of Advanced Materials SPIE 5121, Russian Federation, Moscow, ISBN: 9780819449818 2003, pp. 259–270.

[12] M. Nesladek, A. Bogdan, W. Deferme, N. Tranchant, P. Bergonzo, Charge transport in high mobility single crystal diamond, Diam. Relat. Mater. 17 (2008) 1235–1240.

[13] T.V. Kononenko, V.G. Ralchenko, I.I. Vlasov, S.V. Garnov, V.I. Konov, Ablation of CVD diamond with nanosecond laser pulses of UV-IR range, Diam. Relat. Mater. 7 (1998) 1623–1627.